Acta Materialia 140 (2017) 305–316

Contents lists available at ScienceDirect

Acta Materialia

journal homepage: www.elsevier.com/locate/actamat

Full length article

The interaction of borides and longitudinal twinning in polycrystalline TiAl alloys

Thomas Edward James Edwards*, Fabio Di Gioacchino, Rocío Muñoz-Moreno [1], William John Clegg

Department of Materials Science and Metallurgy, 27 Charles Babbage Rd, University of Cambridge, Cambridge CB3 0FS, UK

ARTICLE INFO

Article history:
Received 25 May 2017
Received in revised form
24 August 2017
Accepted 26 August 2017
Available online 26 August 2017

Keywords:
Titanium aluminides
Deformation twinning
Electron backscattering diffraction (EBSD)
Digital image correlation

ABSTRACT

In this paper the occurrence of twinning parallel to the lamellae during compression at 700 °C of a polycrystalline nearly lamellar commercial γ-TiAl alloy, Ti-45Al-2Nb-2Mn(at%)-0.8 vol% TiB_2, has been studied and shown to lead to the formation of cracks at colony boundaries. However, the occurrence of this longitudinal twinning mode was less common by at least a factor of ten in tests at room temperature. Furthermore, the debonding of colony boundaries caused by the shear strain of longitudinal twinning is exacerbated when the same γ-TiAl variant favourably oriented for twinning occurs repeatedly in the lamellar structure. This effect was caused by the preferential nucleation of certain γ-TiAl variants in the presence of TiB_2 boride reinforcement. It is shown that the boride additions increase the probability of double, triple or even higher order multiply stacked γ-variants. This increases the resulting shear strain that must be accommodated and hence the probability of crack nucleation.

1. Introduction

Though γ titanium aluminides possess a higher specific strength than nickel superalloys [1] at temperatures of the order of 700 °C, they suffer from a sufficient lack of ductility that a threshold approach to fatigue lifing is necessary [2]. Improving the fatigue behaviour of γ-TiAl requires an understanding of crack nucleation and how this is related to the microstructure. To date, much of the work on the deformation modes of TiAl has employed polysynthetically twinned (PST) crystals [3,4] to study dislocation glide and twinning, where the twin-plane is transversal [5] to the lamella interface, *transverse twinning*. In these materials, twinning parallel to the lamellae, *longitudinal twinning*, occurs by the formation of parallel sided twins only ~100 nm in thickness.

Recently, microcompression testing [6] of the polycrystalline commercial alloy, Ti-45Al-2Nb-2Mn(at%)-0.8 vol% TiB_2 (Ti4522XD), where the angle of lamellae to the loading axis was $15° < \Phi < 75°$, *soft-mode*, has shown that longitudinal twinning is also observed. However, its nature is very different to that observed in PST crystals. Unlike the many thin twins [7] of the PST crystals, these longitudinal twins were initiated from the lamellar interfaces and grew across the full width of the lamella. Lamellar domain boundaries were found to impose sufficient constraint to significantly increase the twinning shear stress. The effect of this thicker morphology is to make it difficult to identify a longitudinal twin, as they have straight boundaries and often progress to the completion of a domain. Identifying such longitudinal twins therefore requires that the orientations of the material are known both before and after it has been deformed.

Other techniques, such as SEM *in situ* testing [8] and digital image correlation strain mapping [9], have enabled strain concentrations along TiAl lamellar colony boundaries and cracking along these at high temperature to be observed upon loading. Twinning in equiaxed γ-TiAl grains in duplex TiAl has been reported to generate cracks at grain boundaries as a direct result of the twinning shear [10]. However, due to the difficulties in correctly indexing pseudo-twins, reliable electron backscatter diffraction (EBSD) mapping of tetragonal γ-TiAl for longitudinal twin identification has only become possible [6] due to recent improvements in Kikuchi pattern indexing [11].

* Corresponding author.
E-mail addresses: teje2@cam.ac.uk (T.E.J. Edwards), fd302@cam.ac.uk (F. Di Gioacchino), rocio.munoz@hp.com (R. Muñoz-Moreno), wjc1000@cam.ac.uk (W.J. Clegg).
[1] Present address: HP Inc., Cami de Can Graells, no. 1–21, 08174, Sant Cugat del Valles, Barcelona, Spain.

http://dx.doi.org/10.1016/j.actamat.2017.08.055

1.1. Borides in TiAl alloys

Borides in TiAl [12] are known to reduce texture in polycrystalline alloys. Furthermore, depending on their morphology, they provide some degree of Zener-type pinning which helps refine and stabilize the colony size [13]. A major mechanism for texture reduction is the heterogeneous nucleation of the β- and α-TiAl phases successively on the boride reinforcement during solidification [13], obeying specific crystallographic orientation relationships. Furthermore, there is some evidence of the ability of boride particles to nucleate γ-TiAl [14,15]. In the latter study, the orientation relationship between TiB and γ-TiAl was found to be $\left[0\bar{1}0\right]_{\mathrm{TiB}} \parallel \left[1\bar{1}0\right]_{\gamma}$, $(100)_{\mathrm{TiB}} \parallel \left(11\bar{2}\right)_{\gamma}$. This was considered to be evidence of the nucleation of recrystallising γ-TiAl on TiB. However, it has since been suggested [13] that this relationship might simply result from nucleation of the parent α on TiB, before its Blackburn transformation to γ, which is more widely reported.

This work aims to investigate the effect of boron modification on the distribution of γ-TiAl variants by comparison against a boron-free reference, otherwise of the same composition. The implications of a non-random distribution of γ-TiAl variants on longitudinal twinning-induced colony boundary debonding is investigated in bulk polycrystals of the boron-modified TiAl alloy monotonically deformed at room temperature and 700 °C.

2. Experimental procedures

2.1. Material and metallographic preparation

The TiAl alloy, Ti-45Al-2Nb-2Mn(at%)-0.8 vol% TiB_2 (Ti4522XD), was received as a post-centrifugal casting, which had been hot isostatically pressed at 1250 ± 10 °C for 4 h at a pressure of 140 MPa under an argon atmosphere and then vacuum heat treated at 1010 °C for 8 h, followed by furnace cooling to below 500 °C. This yielded a nearly lamellar microstructure. Alloy compositions measured by AMG Superalloys UK Ltd according to the ASTM standards E2371 (common Ti alloying elements), E1409 (N and O), E1447 (H) and E1941 (C) [16–19] are given in Table 1. Following electro-discharge machining, 4 × 4 × 8 mm^3 cuboids for compression testing, Fig. 1(a), were ground on all faces, with one large face prepared for EBSD mapping by vibratory polishing in a colloidal silica solution for 48 h. An equivalent preparation was employed for the 1 × 2 × 2.5 mm^3 gauge length of tensile test specimens, Fig. 1(b). A second alloy of equivalent composition, but without the boride reinforcement, Ti-45Al-2Nb-2Mn(at%) (Ti4522), was heat treated to an equivalent lamellar thickness to the former by heating at 10 °C min^{-1} to 1350 °C, holding for 30 min and cooling at 2 °C min^{-1}.

2.2. Characterisation of microstructures

Backscatter electron (BSE) imaging in a dual beam FIB/SEM (Helios NanoLab, FEI, USA) enabled colony sizes to be determined using the linear intercept method [20]. Lamellar-scale dimensions and interface types were determined from rectangular strips of lamellar stacks, extracted from EBSD maps obtained on the dual beam FIB/SEM at 20 kV, 6.4 nA, 70° tilt and a working distance of 10 mm, with an EBSD detector and acquisition software (Nordlys-Nano, Oxford Instruments, UK) with the refined accuracy routine [11].

2.3. Mechanical testing

Compression and tensile testing was carried out on a 25 kN screw machine (Tinius Olsen, UK) at a strain rate of 10^{-3} s^{-1}, first to a few percent strain then to just below the buckling limit of the cuboid (~10% strain, exact value dependent on test temperature) in compression. Tensile tests were carried out to failure. Three repeats were performed per condition (25 or 700 °C, compressive or tensile). All samples were mapped by EBSD, but only a subset for each condition had the Au speckle pattern for strain mapping (below) additionally applied.

To avoid significant sample oxidation at 700 °C that would cause Kikuchi patterns to deteriorate and hence impede post-deformation EBSD mapping, a controlled atmosphere chamber was custom built and fitted within the machine, see Fig. 1(c). This enabled Ar pump-purge cleaning and Ti powder gettering at ~700 °C before sample heating using a miniaturised furnace separate to the sample heater; testing was carried out under a vacuum of 10^{-3} mbar or lower. Within this chamber, samples were heated by a resistance heater, stable to ±0.5 °C of the setpoint, based upon a K-type thermocouple either spot welded to a side face of the compression cuboid, or a junction held in contact with the back surface of the tensile testpiece gauge section by a leaf spring to avoid preferentially failing the specimen at the weld point. The system thermally equilibrated until the machine crosshead position drift was significantly below the strain rate.

The experimental setup used did not allow the strain to be measured directly from the sample. Hence for the tensile tests, only stress/displacement curves were plotted.

Before post-test EBSD acquisition, a short polish (<1 min) with water on a chemicloth (MetPrep, UK) following by sonication in acetone was sufficient to remove the majority of any surface deposits, resulting from oxidation, for example.

2.4. Measurement of lamellar orientation and local strain

Fiducial indents were applied to the cuboids and EBSD mapping of the same 230 × 180 μm^2 region containing at least 25 colonies was performed as above with a 200 nm stepsize, both before and after mechanical testing, and sufficiently distant from the plasticity zone of the indents. No fiducials were applied to the tensile specimens to avoid introducing stress concentrators to the sample; the microstructure itself was used as markers. The occurrence of longitudinal twinning was determined from changes in crystal orientation, using a method described elsewhere [6].

For mapping of surface strains by DIC, a remodelled Au speckle

Table 1
Nominal and measured compositions of the two titanium aluminide alloys studied. Note that the boron content in Ti4522XD exceeds the maximum measurable by ASTM E2371.

		Ti/ at.%	Al/ at.%	Nb/ at.%	Mn/ at.%	TiB_2/vol. %	O/ at.%	N/ at.%	C/ at.%	H/ at.%	Mo, Si, Fe, Ni, Cr, W, Co, V, Sn, Bi, Pb, Zr, P/at.%
Ti4522XD	Nominal	bal.	45	2	2	0.8	0	0	0	0	0
	Measured, matrix only (TiB_2 excluded)	bal.	44.7	1.8	1.8	–	0.21	0.05	0.03	0.04	≤0.01
Ti4522	Nominal	bal.	45	2	2	0	0	0	0	0	0
	Measured	bal.	45.3	1.7	1.9	<0.01	0.21	0.02	0.03	0.09	≤0.01

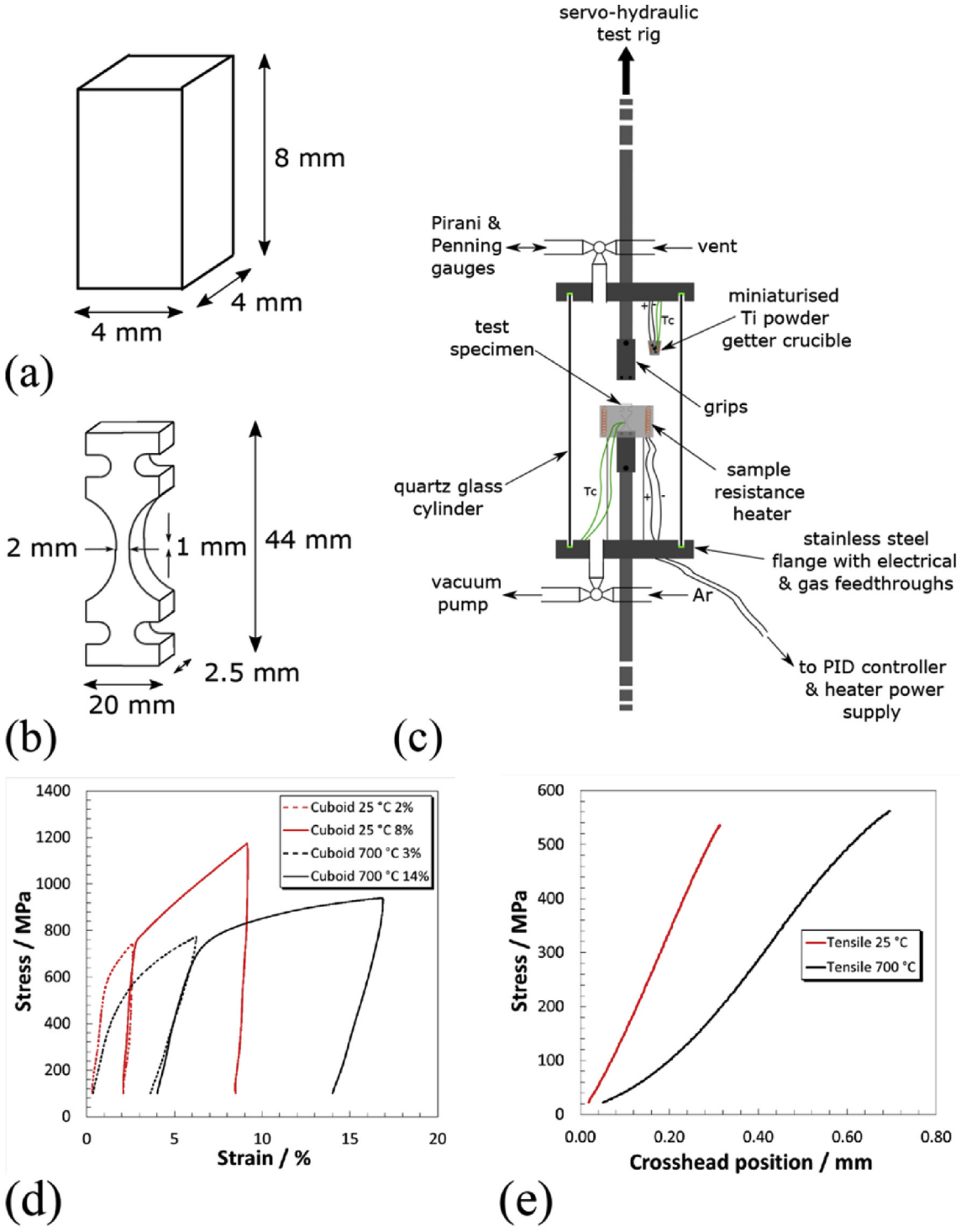

Fig. 1. Diagrams of (a) compression and (b) tensile testpieces, along with the loading curves for both mechanical tests undertaken at room temperature and 700 °C, in (d) compression and (e) tension. (c) schematic of experimental setup.

pattern was applied with a method described elsewhere [21], and imaged at 1500× magnification as a 4 × 4 grid on the dual beam FIB/SEM in high contrast backscatter mode, to be stitched after correlation. Image correlation of pre- and post-deformation SEM images was performed on commercially available DIC software (DaVis, LaVision, Germany), with a subset size of 8 × 8 pixels and 25% overlap, which gave a resolution of ~180 × 180 nm^2.

2.5. Determination of the probability for random stacking of γ-TiAl lamellae

The calculation of the theoretical, random reference is based upon a six-sided repeated dice-roll model simulated using a random number generator in a commercial software package (Matlab, Mathworks, USA). The simulation converged to 4

significant figures for both the averages and standard deviations of the stacking probabilities after one million repeats of the repeated dice-roll.

3. Results

3.1. Compression testing

The two stage compression testing of Ti4522XD cuboids at 700 °C and at room temperature resulted in the successive EBSD maps presented in Figs. 2 and 3, and 4, respectively, along with the loading curves, corrected for rig compliance, Fig. 1(d). The initial microstructures of the regions of interest are given as backscattered electron images, Fig. 5(a and b).

The custom-built controlled atmosphere chamber was successful in maintaining sufficiently low oxidation rates of the sample surface at 700 °C for the majority of the region in the post-test EBSD maps, Fig. 2(b and c), to produce clear Kikuchi patterns of the base material and index well. There is some localised deterioration in the indexing, indicated as regions of white datapoints, despite the significant efforts. The indexing of minority phase α_2-Ti_3Al is the more variable. In contrast, at room temperature, even by 8% compression, Fig. 3(c), there is little reduction in the quality of the EBSD pattern.

The occurrence of longitudinal twinning at 700 °C was identified by very specific crystal orientation changes characteristic of such twinning mode [6] and, hence, by the specific colour changes indicated in the reduced area Fig. 2. Lamellae undergoing such twinning are arrowed in each testing step. Longitudinal twinning had initiated by a compressive strain of 3%, Fig. 2(b,e). The transformation continued as the strain increased from 3% to 14%, so that the twins had grown across the full width of the original lamellae, and they were hence parallel sided. In locating and following specific γ-TiAl lamellae, the α_2-Ti_3Al lamellae were used as reference markers as these remain orientation invariant, apart from small amounts of stress-induced bending.

In fact, longitudinal twinning in compression was observed to have been operative in all soft-mode oriented colonies studied at 700 °C, as indicated by arrowed lamellae in Fig. 3(a–c); in total, 107 lamellae underwent longitudinal twinning. Generally, the only twinning-active γ-variant per colony was that with the highest Schmid factor for longitudinal twinning. However in the case of colony 1 of Fig. 3(a), for example, two γ-variants are activated and possess similar such Schmid factors: 0.360_C and 0.341_C. Longitudinal twinning was not observed in hard-mode colonies, e.g. colony 4, Fig. 3.

At room temperature, longitudinal deformation twinning in compression was found to operate to a much lesser extent, Fig. 4, even after the second loading step. Fewer lamellae per colony were observed to twin, by at least a factor of ten. The twinned material often contacted an interface of the parent lamella, similarly as for longitudinal twins at 700 °C.

Further analysis was undertaken on the post-deformation EBSD maps to reveal the extent of bending of lamellae by changes in the lattice orientation along their lengths; the graphs in Fig. 6(a and b) show variations in misorientation along lines indicated on the EBSD maps, Figs. 3(c) and 4(c), relative to the midpoint of the lamellae. Despite a considerably lower final strain imposed at room temperature, rotations over 10° along lamellae were often obtained, whereas at 700 °C rotations rarely exceeded 5°.

The curvature along lamellae, particularly at 25 °C, was not constant, but had a maximum value close to the colony boundaries, with large rotation gradients of 5° occurring over a distance of 2 μm, Fig. 6(b). This is also seen in kernel average misorientation (KAM) maps using a 5 × 5 datapoint circular filter, inset in Fig. 4(c). These show the average misorientation that each pixel has with its neighbours. These show maxima at the ends of lamellar domains adjoining colony boundaries. An additional feature of such maps are sets of parallel bands of high KAM that lie transverse to lamellae at room temperature, Fig. 4(c), in distinctly crystallographic orientations (along the {111} plane traces). These may be compared with band contrast (image quality) and mean angular deviation (MAD) maps of the same sub-regions, Fig. 4(c). In both these data acquisition and indexing quality maps, respectively, such transverse bands are also explicited. There is no evidence in the crystal orientation maps that these bands are caused by transverse twins.

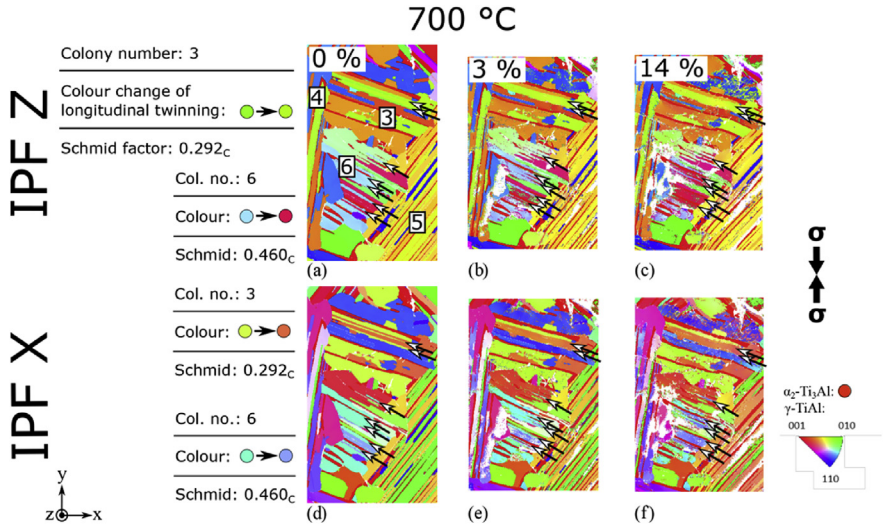

Fig. 2. Crystal orientation maps obtained by electron backscatter diffraction of a reduced region of Fig. 3, after compression stages of 0, 3 and 14% strain, respectively, of a Ti-45Al-2Nb-2Mn(at%)-0.8 vol% TiB_2 cuboid at 700 °C. (a–c) are given in inverse pole figure colouring with respect to the z-axis (IPF-Z), and (d–f) are in IPF-X colouring; this enables better distinction of twins where parent and twin orientations are represented by similar colours in one colouring scheme. Arrows in black with hollow ends locate the longitudinal twins apparent by the final compression step. The colour changes associated with the lattice orientation changes upon longitudinal twinning are indicated in the figure surround per numbered colony, along with the Schmid factor for operation of the relevant twin system (subscripts T and C indicate operability of the twin in tension and compression, respectively). Datapoints in white are non-indexed, mainly due to localised oxidation effects. (For interpretation of the references to colour in this figure legend, the reader is referred to the web version of this article.)

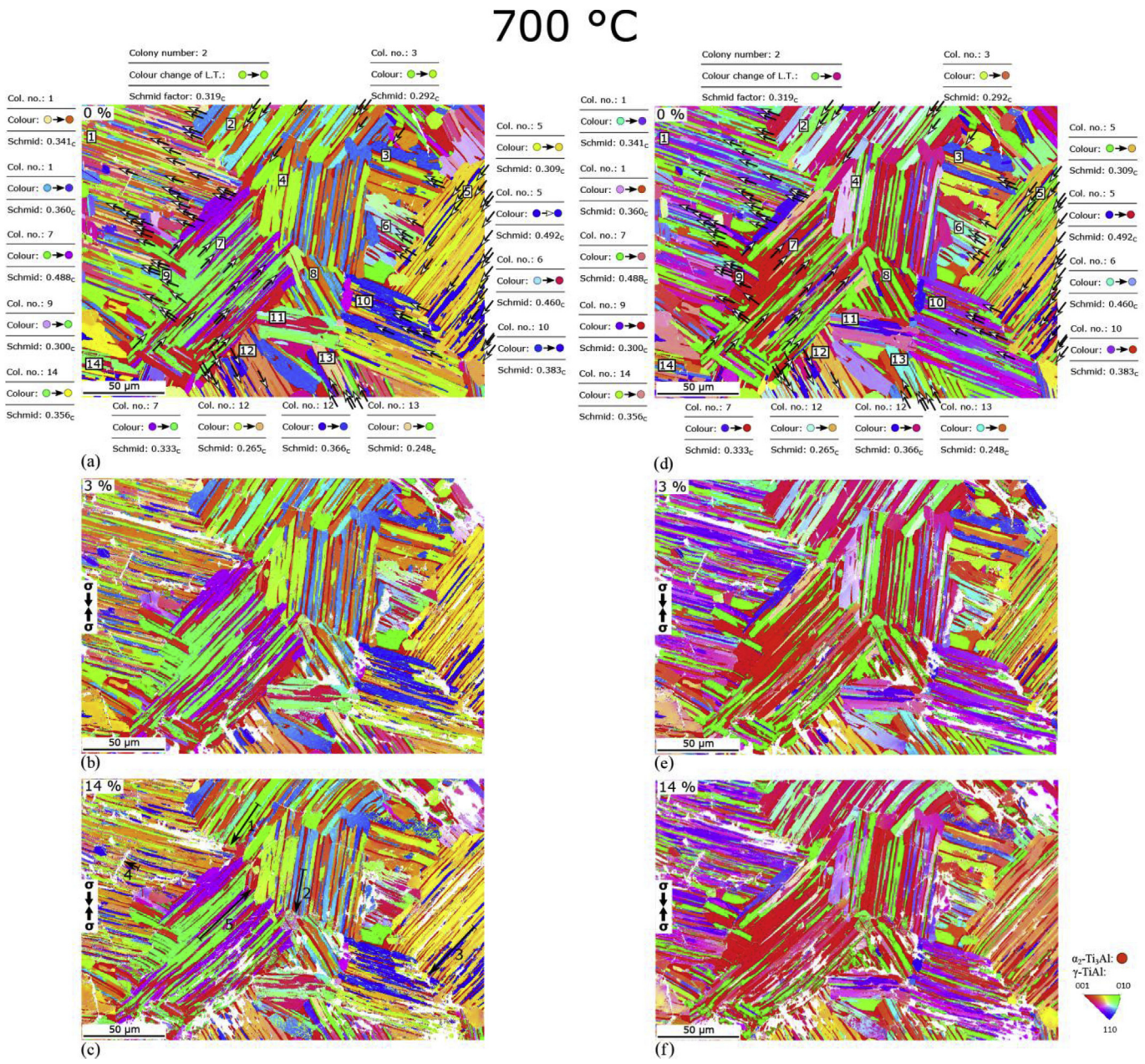

Fig. 3. (a–c) are crystal orientation maps obtained by electron backscatter diffraction of the same region of a Ti-45Al-2Nb-2Mn(at%)-0.8 vol% TiB_2 cuboid, captured at compression stages of 0, 3 and 14% strain, respectively, at 700 °C. The colour convention is IPF-Z, all annotations carry the same meaning as in Fig. 2. (d–f) are identical orientation maps to (a–c) but are given in the IPF-X colouring convention. Arrows in black in (c) locate the misorientation lineplots in Fig. 6(a). (For interpretation of the references to colour in this figure legend, the reader is referred to the web version of this article.)

However this cannot be ruled out as the twins may be sufficiently thin that they could not be detected at the 200 nm scan stepsize. At 700 °C, in colony 1 the local bending of matrix lamellae around an intra-colonial boride is shown, Fig. 3(c). Local bending in excess of 10° of both the γ-TiAl and α_2-Ti_3Al lamellae either side of this elongated hard particle is well described by the misorientation line plots, Fig. 6(a).

The locations of cracks forming in compression were determined by backscatter electron imaging of the regions of interest. The locations of all the flaws identified are indicated in Fig. 5(a and b), along with their type. For the 700 °C tested sample, many cracks were found in the proximity of borides, along the boride-matrix interfaces, Fig. 5(a); borides also cracked transverse to their length. Elsewhere, much colony boundary debonding was observed, Fig. 5(a); in all cases where this was not associated with a colony boundary boride, the flaws were found to be adjacent to a longitudinal deformation twin, as identified above. At 700 °C, this was the case for 9% of the lamellae that twinned longitudinally and also reached a colony boundary within the plane scanned in Fig. 3. Interlamellar debonding was occasionally observed, outside of the current region of interest. Cracking in the room temperature tested cuboid was more varied, Fig. 5(b): similar boride cracking characteristics were observed as with high temperature testing. However, colony boundary failure was not solely associated with longitudinal twinning; 50% of the lamellae that twinned longitudinally at 25 °C were associated with colony boundary debonding, however, the occurrence of longitudinal twinning was too low for this value to be significant. In some cases boundary flaws were found ahead of α_2-

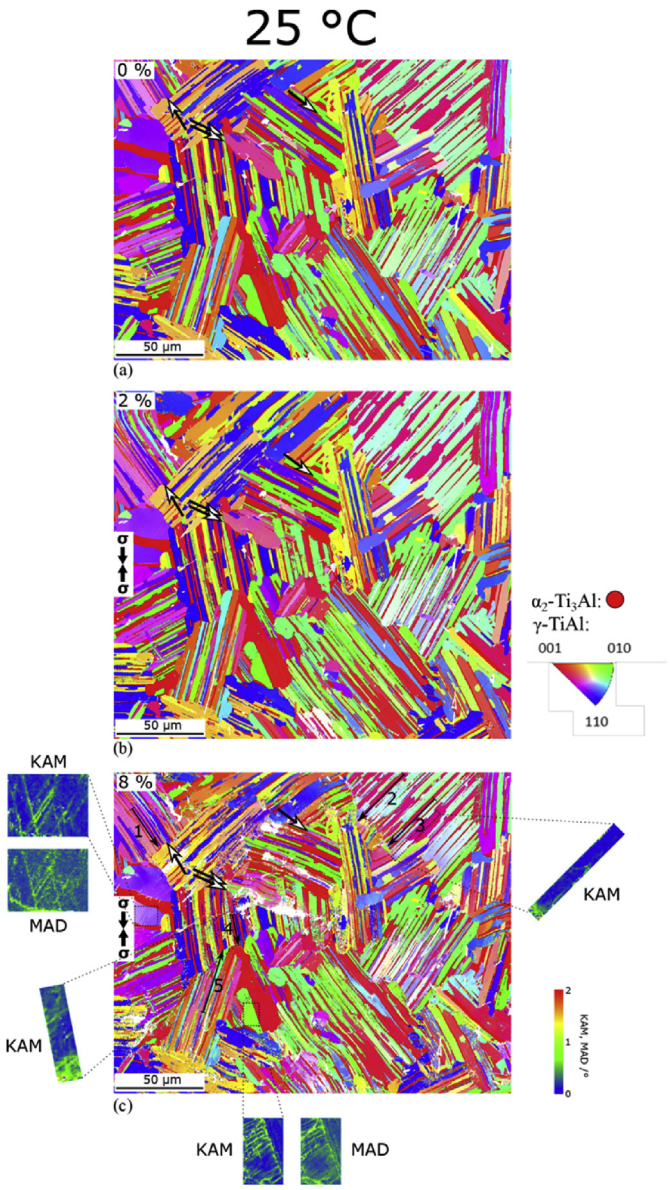

Fig. 4. (a–c) are crystal orientation maps obtained by electron backscatter diffraction of the same region of a Ti-45Al-2Nb-2Mn(at%)-0.8 vol% TiB_2 cuboid, after compression to 0, 2 and 8% strain, respectively, at room temperature. The colour convention is IPF-Z. Arrows in black with hollow ends locate the longitudinal twins apparent by the final compression step. Regions of high lattice rotation at the ends of lamellae, near the colony boundary, are noted in (c) insets by peaks in the kernel average misorientation (KAM). Furthermore, bands within lamellae, transverse to their long axis, are observed both in KAM and mean angular deviation (MAD) maps. (For interpretation of the references to colour in this figure legend, the reader is referred to the web version of this article.)

Ti_3Al lamellae, insets Fig. 5(b), or along colony boundaries where the neighbouring lamellae had undergone considerable bending, Figs. 4(c), 5(b) and 6(b).

3.1.1. DIC strain mapping of deformation in compression

Surface strain mapping by DIC of deformation in compression of soft-mode oriented colonies at 700 °C revealed wide bands of deformation, Fig. 7(a, c), coincident and consistent with lamellae undergoing longitudinal twinning. These deformation twins were evidenced similarly as above, by crystal orientation changes in the EBSD maps, Fig. 7(b, d). Note that the α_2-Ti_3Al phase in particular does not index as well, a feature arising from the DIC patterning process. Such wide bands of deformation contrast with the fine shear bands parallel to the lamellar interfaces in lamellae where longitudinal and mixed-type [5] dislocation motion had occurred due to a higher Schmid factor than for twinning in those specific γ-variants.

In this case, the insets, Fig. 7(d), show that colony boundary cracking occurs ahead of the longitudinal twins at 700 °C. The effect of domain boundaries between γ-TiAl order variants within a same lamella on the distribution of strain is highlighted in Fig. 7(c) where the large twinning shear is halted, and propagated into the γ-TiAl order variant ahead as multiple diminishing microslip bands. Unlike the colony boundary, secondary electron imaging of the domain boundary revealed no debonding.

3.2. Tensile testing

As expected, the tensile failure strains at both room temperature and 700 °C were less in tension than in compression, Fig. 1(e). In all specimens the mapped regions within the gauge length, Fig. 8(a,d), were at a considerable distance (>300 μm) from the primary crack. Although longitudinal deformation twinning occurred on tensile testing at 700 °C, Fig. 8(b and c), it was much less common than in compression tests at 700 °C. Elsewhere, at room temperature, comparison of the pre- and post-tensile deformation crystal orientation maps, Fig. 8(e and f), did not reveal the occurrence of longitudinal twinning, though the macroscopic strain achieved was also the lowest of all the tests in the current work.

Backscatter electron imaging of the tensile specimens after loading to fracture identified similar flaw locations to compression testing, with colony boundary debonding ahead of α_2-Ti_3Al lamellae being a staple at both test temperatures, along with the cracking of many borides and their debonding from the matrix. Furthermore, transverse boride cracking was found to propagate into the surrounding lamellar γ-TiAl matrix, Fig. 9(a and b), particularly at 25 °C.

3.3. Effect of borides on the stacking sequence of γ-variants

To demonstrate the effect of titanium diboride on the distribution of γ-variants, two alloy compositions were considered: Ti4522XD and Ti4522, with and without boride additions respectively, and otherwise identical in composition. The boron-free Ti4522 was solution treated at 1350 °C for 0.5 h followed by a slow cool at 2 °C min^{-1} in order to grow lamellae of similar dimensions to those in the Ti4522XD, Table 2. The slow cool and the absence of the boride pinning of colony boundaries led to the colony size increasing to above 2 mm.

EBSD maps of the lamellar stacking in Ti4522 were acquired from three colonies, as in Fig. 10(a), such that a total of 350 lamellae (101 α_2-Ti_3Al lamellae) were characterized; the measured indicator was the nature of γ-variants (γ_1, γ_2, γ_3, γ_{1T}, γ_{2T}, γ_{3T}, as per [7]) on either side of the α_2 lamellae. Such γ-variants could either be simply different (e.g. $\gamma_1/\alpha_2/\gamma_2$), the same (e.g. $\gamma_1/\alpha_2/\gamma_1$ 'double' stacking) or even higher order repeated stacking (e.g. $\gamma_1/\alpha_2/\gamma_1/\alpha_2/\gamma_1$ 'triple' stacking). Hence a histogram, Fig. 10(c), of the occurrence frequencies was produced, where a theoretical, random reference is also plotted. From this, it was determined that to within the average deviation for a finite number of counts, the boride-free material displays a random spread of γ-variant stacking on either side of α_2 lamellae.

However, an analysis of 166 lamellae of the boron-modified material, from strips as in Fig. 10(b), reveals an increase, in particular, in the number of triple-type repeated stacking compared to the boron-free material, Fig. 10(c), well beyond the 99th percentile

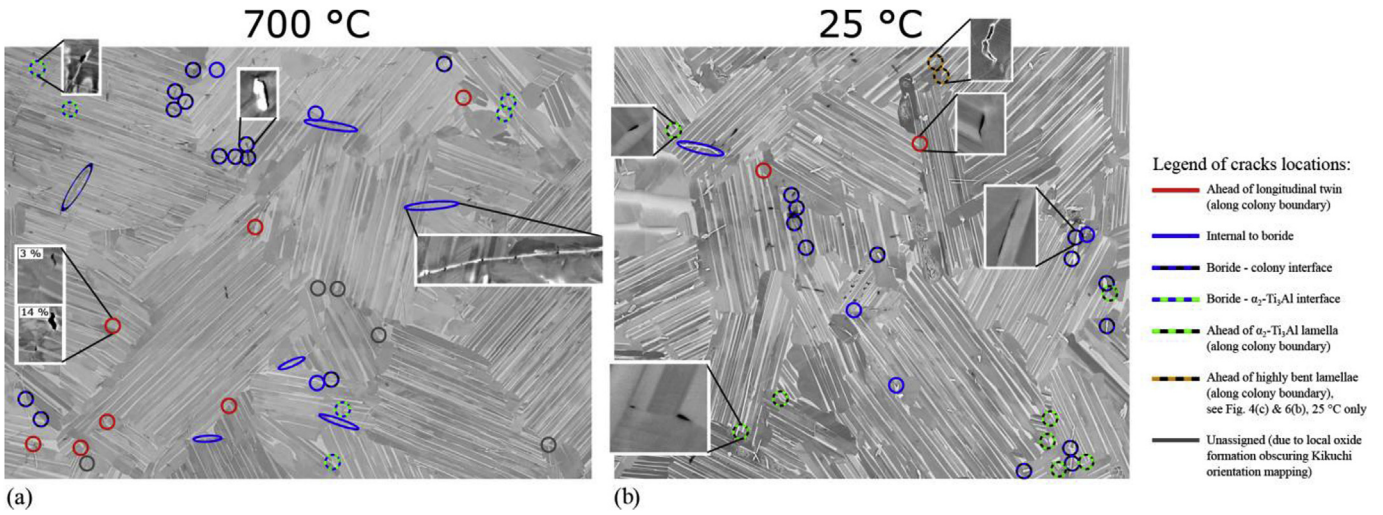

Fig. 5. Backscatter electron images of the unstrained regions of interest in compression specimens of Ti-45Al-2Nb-2Mn(at%)-0.8 vol% TiB_2 tested at (a) 700 °C and (b) 25 °C. The locations of cracks developed upon compression are circled; characteristic examples of each flaw location are given as insets. At 700 °C, colony boundary debonding was consistently adjacent to lamellae having undergone longitudinal twinning, when not related to borides.

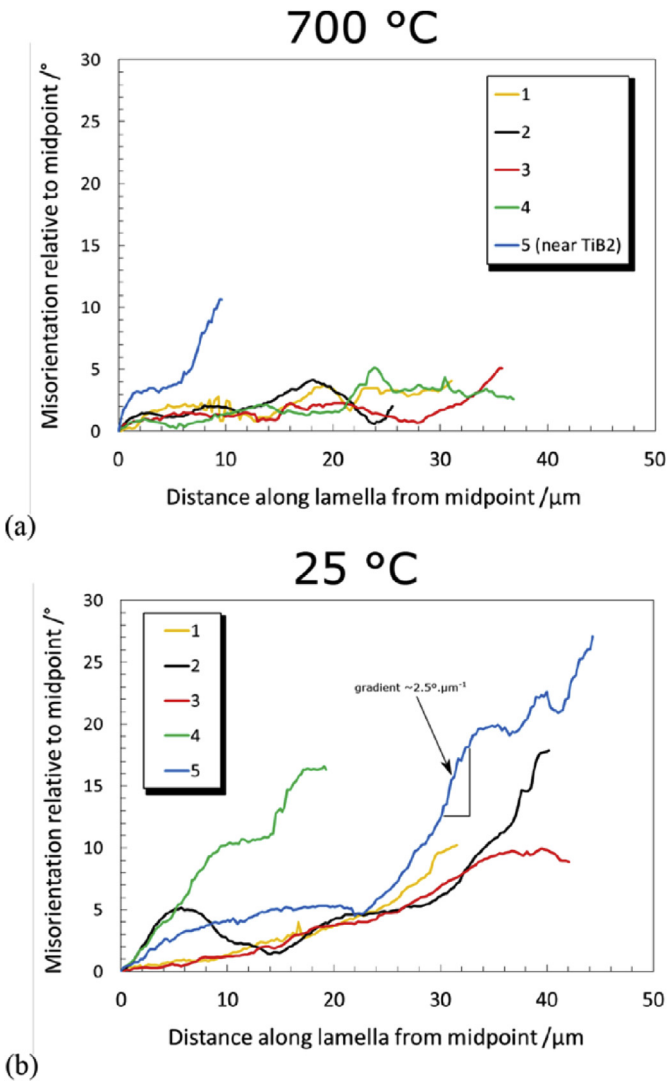

Fig. 6. Plots of misorientation angles along lamellae after compression testing at (a) 700 °C and (b) 25 °C. Lineplots are numerically identified in Figs. 3(c) and 4(c), respectively.

of random selection of γ-variant stacking. That is to say, the stacking of γ-TiAl variants with respect to the α_2-Ti_3Al lamellae in the boron-modified Ti4522XD alloy is definitely non-random.

4. Discussion

4.1. Operation of longitudinal twinning

Direct evidence is provided in section 3.1 for the operation of longitudinal twinning in a polycrystalline titanium aluminide alloy of commercial interest at aero-engine operational temperatures. This required a test chamber that ensured sufficiently low oxidation rates of the TiAl testpieces such that an EBSD-suitable surface polish could be maintained throughout the mechanical test schedule. There was difficulty in indexing the patterns in some small regions, associated with local surface oxidation giving rise to poorer pattern quality at 700 °C, Fig. 2(c). This meant that longitudinal twinning could sometimes not be unambiguously identified in these regions, as for colony 8 in Fig. 3(c). Due to the exclusion of such regions, the frequency of twinning reported at 700 °C should therefore be taken as a lower bound.

The observation that such longitudinal twinning occurs more extensively at 700 °C relative to room temperature, at least on the sample surface, may be compared with the results of a recent microcompression study of longitudinal twinning in the same alloy [6]. At room temperature, longitudinal twinning operated in soft-mode oriented micropillars, in every Schmid-preferred lamella, at a resolved shear stress of 100 MPa, lower than that for both $<1\bar{1}0]\{111\}$ ordinary and $<\bar{1}01]\{111\}$ super-dislocation mechanisms [22]. However, it was further noted that the introduction of a domain boundary, that is the interface between two γ-TiAl order variants within a same lamella, significantly raised the twinning shear stress [6], similarly to [23]. This indicates that the geometric constraint in the polycrystal contributes to the hindering of longitudinal twinning, which is in agreement with its reduced extent of operation at room temperature in the current work. Further microcompression experiments at 700 °C are required to characterise completely the temperature dependence of the ease of longitudinal twinning.

The current study measures the occurrence of longitudinal twinning of γ-TiAl on the sample surface. Crystal plasticity

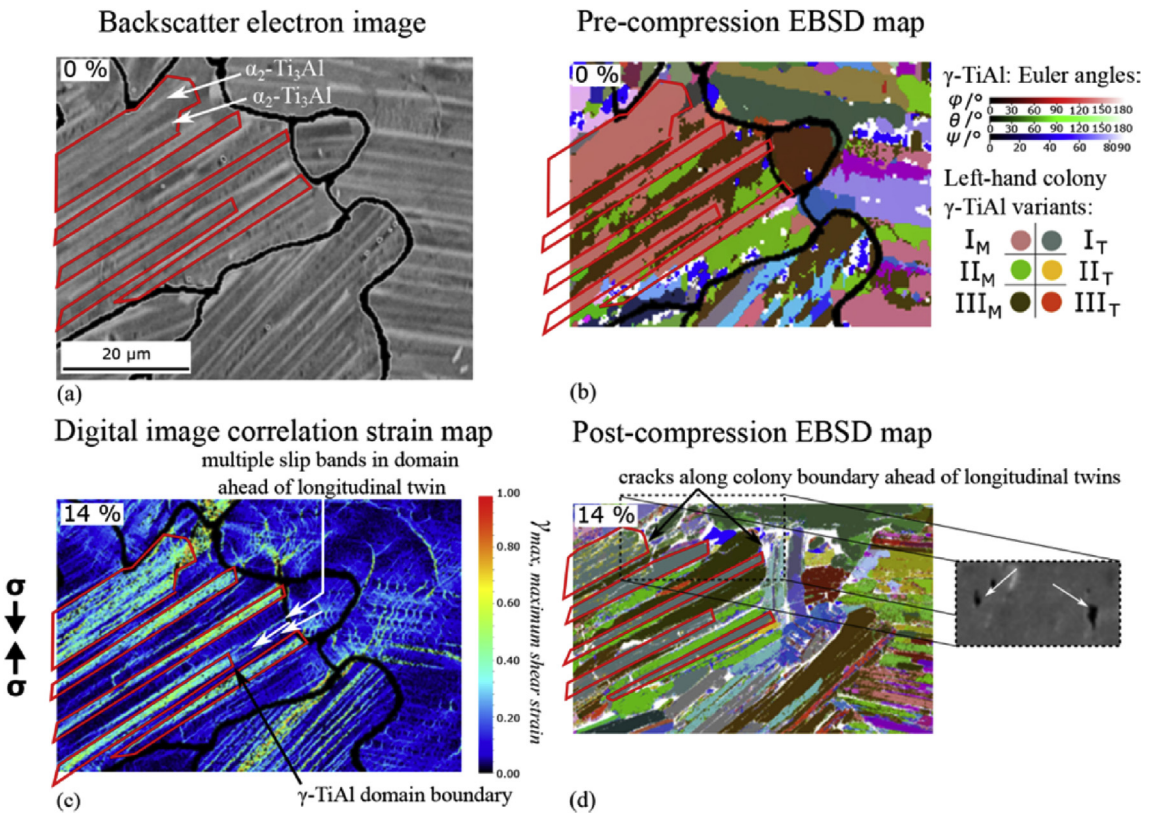

Fig. 7. Combined (b) digital image correlation strain mapping and (c,d) electron backscatter diffraction orientation mapping results of the region of a Ti-45Al-2Nb-2Mn(at%)-0.8 vol % TiB_2 cuboid electron backscatter imaged in (a) that underwent compression to 14% at 700 °C. The dissipation of the twinning shear strain is ensured by multiple slip bands ahead of a domain boundary; such slip bands are arrowed in (b). Cracks developed ahead of the longitudinally twinned lamellae are displayed in insets, particularly ahead of a 'multiply stacked' set of γ-TiAl lamellae, arrowed in (c,d). Poor indexing of the α_2-Ti_3Al phase results from the Au speckling process; these lamellae may be identified by the lighter contrast in (a).

modelling [24] has demonstrated that the stress state in a lamellar colony at a free surface is different to that in a colony embedded within the specimen, due to the differences in the proportion of a colony that experiences the constraint of neighbouring colonies. Further, such free surfaces were found [24] to reduce the strain-hardening rate, and more so when the colony size increases, or the sample size decreases. However, it is difficult to confirm the operation of longitudinal twinning in the bulk, where the constraint of surrounding material may be sufficient to resist the twinning shear and thereby impede the operation of mechanical twinning. Nevertheless, the observation of longitudinal twin formation at a surface, and its association with crack formation, is relevant in light of the importance of surface nucleation of cracks in the fracture and fatigue failure of γ-TiAl alloys [25].

The progression of longitudinal twinning at 700 °C between 3% and 14% strain steps is identical to observations of interrupted tests in the micropillar study [6], in that incomplete twins consistently contact lamellar boundaries, suggesting nucleation on these interfaces, as previously remarked [26]. The few occurrences of longitudinal twinning at room temperature similarly contact lamellar boundaries and hence also agree with the above mechanism. The fact that this twinning mechanism is rapidly exhausted indicates its limited benefit in ensuring continuous plasticity in response to loading [27]. Furthermore, as in the micropillar testing, longitudinal twinning in the polycrystalline material here maintains parallel boundaries: the whole lamella twins [6] rather than forming a tip strain-relieving lenticular deformation twin [28]. As a result, the full twinning shear must be accommodated ahead of the twin. As previously reported [6], such twinning is halted by domain boundaries, with a diminishing extent of slip measured by strain mapping in the neighbouring domain, ensuring boundary cohesion, similarly noted here in Fig. 7. In contrast, at colony boundaries, there is evidence here for crack nucleation resulting from an opening stress due to the twinning shear, Fig. 4(c), both from the shapes of cracks and the consistent spatial association of colony boundary cracks and longitudinal twins, particularly at 700 °C. Such twinning-induced boundary decohesion is reported for equiaxed γ-TiAl grains at room temperature in Ti-48Al-2Nb-2Cr (at.%) [10]. Features near the fracture surface of the third generation alloy Ti-43.5Al-4Nb-1Mo-0.1B (at.%) [29] were similarly reported as γ-TiAl mechanical twins. Depending on whether such twins were located ahead of the growing primary crack or in its wake, they caused either intergranular microcracking or acted as a crack-shielding mechanism, respectively.

The results of tensile testing serve to confirm the compression observations that the longitudinal deformation twinning of polycrystalline Ti4522XD occurs at 700 °C. The fact that less longitudinal deformation twins are found to operate in tension is consistent with the significantly reduced macrostrain imposed in comparison to the compression tests. The potential for the production of colony boundary flaws ahead of the longitudinal twins is significant in light of the importance of the cracking of colony boundaries in the eventual failure of this alloy at high temperature. Work elsewhere on this alloy [8] has similarly identified colony boundary cracking at the same temperature and strain rate.

The increased amount of rotation of lamellae in the colony boundary regions at room temperature, even at lower overall macrostrains, suggests a change in the relative ease of activation of

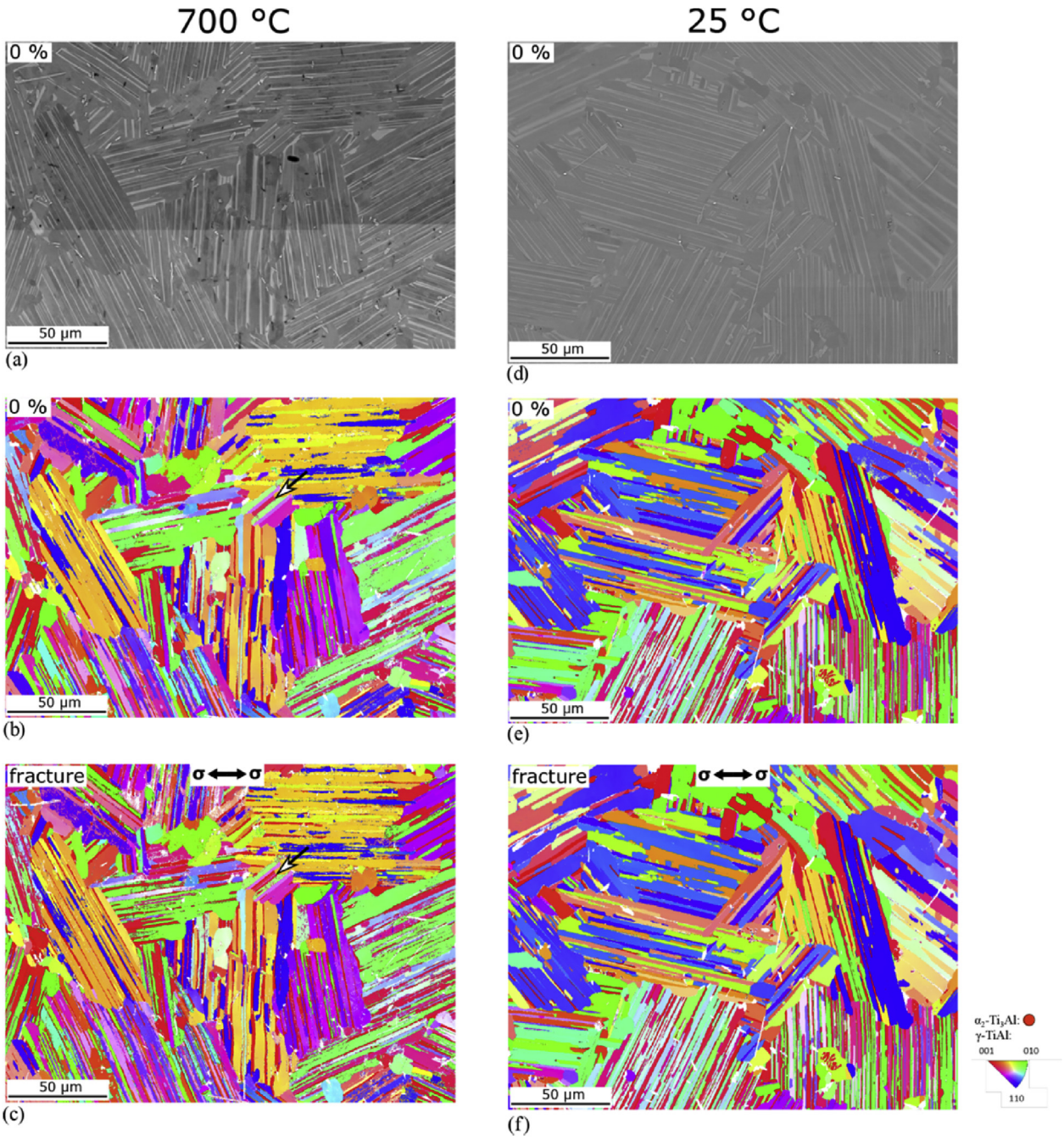

Fig. 8. Backscatter electron images of the regions of interest in tensile specimens of Ti-45Al-2Nb-2Mn(at%)-0.8 vol% TiB_2 before testing at (a) 700 °C and (d) 25 °C, along with the crystal orientation maps of these regions (b,e) before testing and (c,f) after specimen fracture. Locations where longitudinal twinning was identified to have occurred in tension are annotated in an equivalent manner to the compression data in Fig. 2.

the different deformation mechanisms compared to 700 °C. This lattice curvature requires an increased elastic energy storage at room temperature to accommodate deformation between neighbouring colonies, with or without the presence of geometrically necessary dislocations (GNDs) [30]. Such stored elastic energy may also drive boundary failure. This is consistent with the present observation of flaws ahead of intensely locally rotated γ-TiAl lamellae.

In addition, the observation of colony boundary decohesion ahead of wide lamellae of the harder α_2-Ti_3Al phase should similarly not be overlooked, but rather further investigated as a potential fatigue microcrack nucleator.

4.2. Role of borides in TiAl alloys

The differences in distribution of the γ-variants on either side of the α_2 lamellae in the presence and absence of boron modification observed in the current study, Fig. 9(c), indicates that titanium borides influence the nucleation of γ-TiAl upon cooling from the α-TiAl single phase region. Specifically, the boride particles cause a spatial preference for the nucleation of certain γ-TiAl variants whereby the same γ-TiAl variant is grown in repeated succession in one part of a lamellar colony, with the γ-TiAl lamellae finally separated only by fine lamellae of the remaining parent α_2-Ti_3Al. In a given colony and along its boundaries, the number of borides is

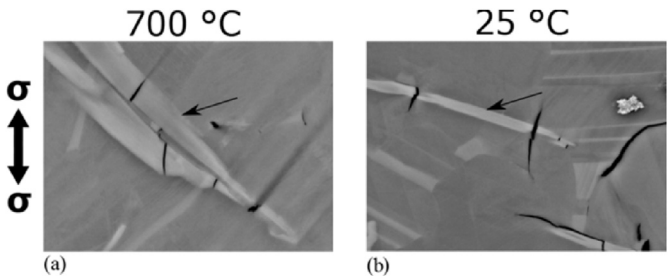

Fig. 9. Backscatter electron images of cracked boride particles in Ti4522XD tested in tension to fracture at (a) 700 °C and (b) 25 °C.

$O(10^2–10^3)$, depending on the predominant boride morphology – flaky or bar – in the region of the Ti4522XD material considered. With such a large number of boride particles, it is a difficult task to identify the particular boride responsible for the repeated occurrence of a certain γ-TiAl variant in a particular spatial region. And this, not in the least because the boride of interest may well have been removed during the EDM, grinding and polishing steps of sample preparation. It is therefore not possible to determine a mechanism by which this spatial preference occurs, such as a crystallographic relationship between the boride and the locally predominant γ-variant that might evidence coherent heterogenerous precipitation of the γ-variant on the boride.

The increased frequency of double, triple, or even higher order, stacking of identical γ-variants either side of the α_2 lamellae, caused by boride additions, is of considerable concern for the longitudinal deformation twinning. Under the assumption of the relative plastic inactivity of the harder α_2-Ti_3Al layers [2], the cumulative twinning shear of this multiple stacking of an identical γ-variant can be very large, as illustrated in Fig. 11, which may increase the Mode I crack opening stress on the colony boundary. This is, for example, observed in Fig. 7 where colony boundary cracks have formed ahead of both double and triple identical γ-variant stacks.

In short, boride additions raise the risk of the preferentially

Table 2
Microstructural parameters of Ti-45Al-2Nb-2Mn(at%)-0.8 vol% TiB_2 (Ti4522XD) and Ti-45Al-2Nb-2Mn(at%) (Ti4522) alloys obtained from BSE images (colony size) and EBSD maps (lamellar dimensions).

Alloy	α_2 fraction	Colony size/μm	Mean γ lamellar thickness/μm	Mean α_2 lamellar thickness/μm
Ti4522XD	9.5%	70	1.4 ± 0.9	0.26 ± 0.09
Ti4522	23.3%	>2000	0.68 ± 0.76	0.58 ± 0.50

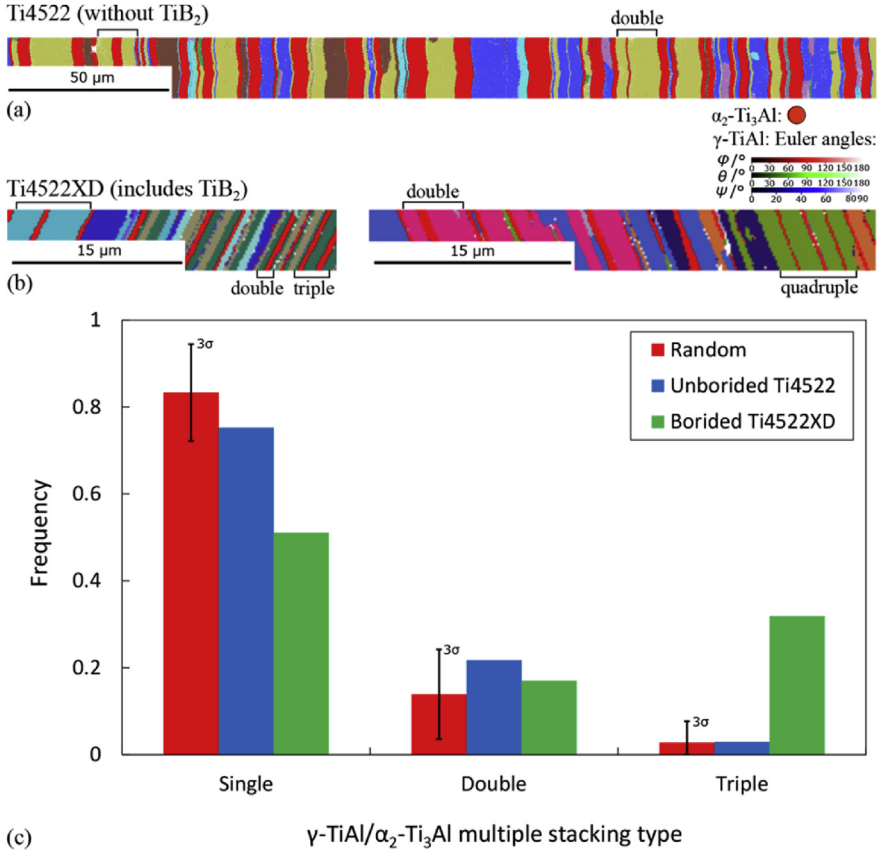

Fig. 10. Examples of crystal orientation mapping strips from individual colonies obtained by EBSD for (a) the boron-free Ti-45Al-2Nb-2Mn(at%) alloy (at a 40 nm stepsize) and (b) the boride-reinforced Ti-45Al-2Nb-2Mn(at%)-0.8 vol% TiB_2 (as above) in order to determine (c) the distribution of lamellar stacking types: 'single', 'double' or 'triple', as described in the section and indicated in (a,b). Higher order stacking repeats were collapsed into the 'triple' category for simplicity, without loss of meaningfulness of the results. The average and 3σ of the occurrence of the stacking types based on sampling 101 α_2-Ti_3Al lamellae from a simulated random distribution of γ-TiAl lamellae either side of the α_2-Ti_3Al are also reported.

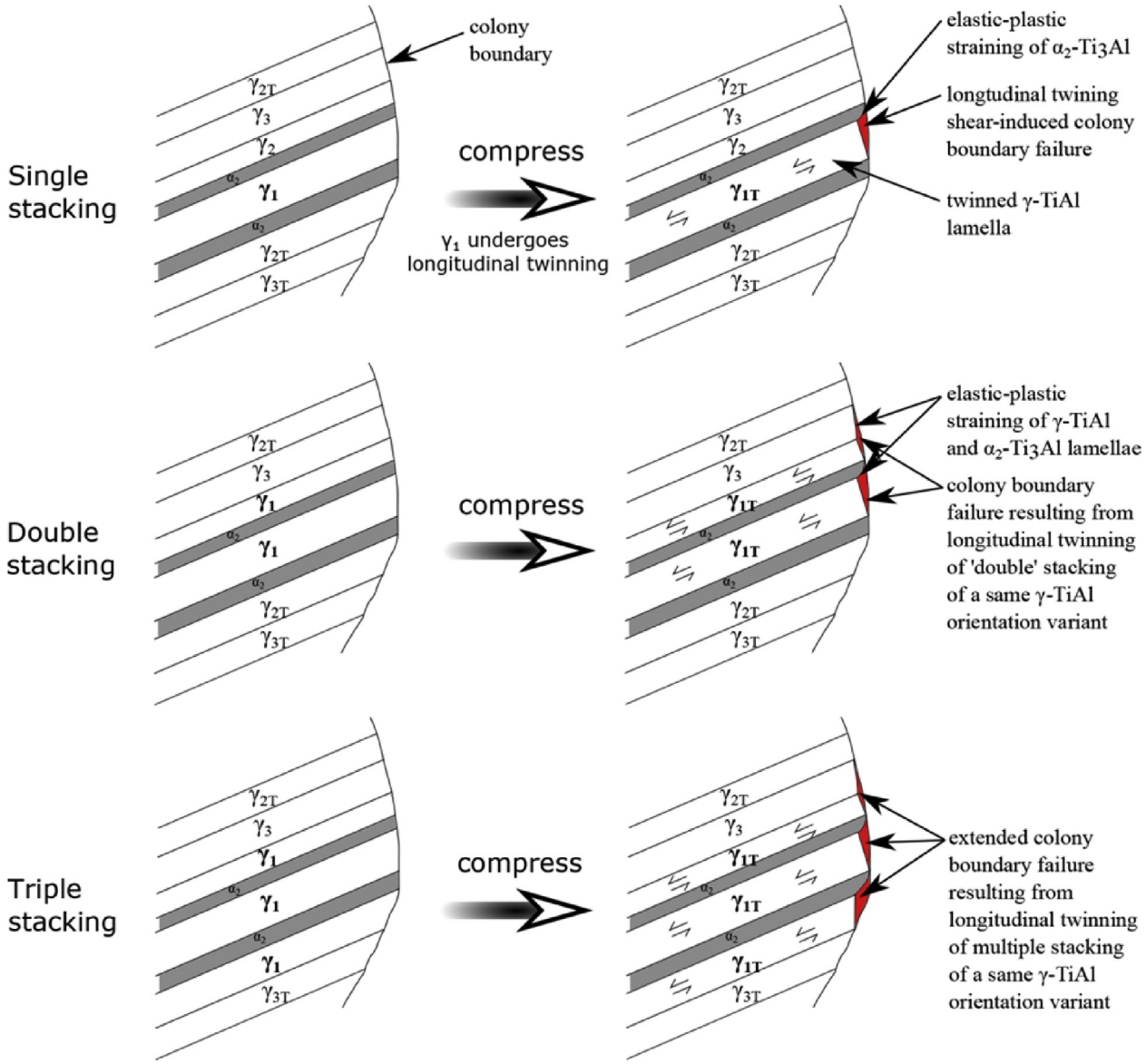

Fig. 11. Diagrammatic of the multiple stacking concept, highlighting the extended colony boundary decohesion resulting from the shear of longitudinal twinning of multiply stacked identical γ-TiAl orientation variants, the existence of which is found to be associated with the presence of TiB_2 particles in the alloy.

oriented γ-variant for longitudinal deformation twinning in a soft-mode colony occurring as a doubly or, worse, triply stacked group, and hence generating a large, potentially colony boundary-failing, twinning shear.

It was not possible to comparatively test the effect of the presence and absence in the Ti4522XD and Ti4522 alloys, respectively, of such multiply-stacked identical γ-variants, and the longitudinal twinning thereof, on the room and high temperature ductility. This was because the heat treatments necessary to develop sufficiently thick lamellae for crystal orientation mapping by EBSD also produced very large colonies (>2 mm in diameter) in the boron-free material, compared to the boron-modified material (70 μm). Such a large change in the colony size parameter would significantly affect the mechanical properties, based on results by Cao et al. [31] where the influence of the lamellar colony size on the loading behaviour was noted even for a much lesser relative variation in colony size than here. Hence it would not be possible to extract the specific effect of the reduced occurrence of multiply-stacked lamellae.

Finally, it has been reported that the fracture of boride reinforcement, or debonding along the interfaces of such hard particles with the TiAl matrix, is not a cause for fatigue crack nucleation [32]. Rather, it is thought, such boride cracking only populates the final fracture surface during later stages of crack growth. The results from the current monotonic loading work, and other recent studies [8], indicate that transversal boride cracks propagate out into the surrounding lamellar matrix and along colony boundaries at 25 °C and 700 °C. Given the importance of microcracks on the fatigue life of titanium aluminide alloys [33], the effect of such borides on the nucleation, rather than just the propagation, of fine flaws during cyclic sub-yield loading requires further study.

5. Conclusions

The present work has directly identified the occurrence of longitudinal twinning of the surface of polycrystals of Ti-45Al-2Nb-2Mn(at%)-0.8 vol% TiB_2 upon loading in both compression and tension at 700 °C, and the lesser operation of such deformation

mode at room temperature. Cracks at lamellar colony boundaries were found to be consistently associated with such longitudinal twins, particularly at 700 °C, with colony boundaries being the major initial and secondary cracking path in the material at that temperature. The boride reinforcement causes localised preferential nucleation of certain γ-variants. This results in a much larger cumulative twinning shear to be accommodated at colony boundaries, increasing the risk of twinning-induced boundary decohesion.

Acknowledgements

The work was supported by the EPSRC/Rolls-Royce Strategic Partnership (EP/M005607/1). We kindly acknowledge Dawei Hu for providing the boron-free Ti4522 material. Robert Stearn is acknowledged for his help in the construction of the controlled atmosphere test chamber. Richard Langford is acknowledged for his help in establishing and sustaining EBSD equipment capability for TiAl alloys. Thanks are due to Nigel Martin (Rolls-Royce plc) for obtaining bulk compositions of the alloys studied.

References

[1] H. Clemens, H. Kestler, Processing and applications of intermetallic γ-TiAl-based alloys, Adv. Eng. Mater. 2 (9) (2000) 551–570.
[2] F. Appel, J.D.H. Paul, M. Oehring, Gamma Titanium Aluminide Alloys : Science and Technology, Wiley-VCH, Weinheim, 2011.
[3] T. Fujiwara, A. Nakamura, M. Hosomi, S.R. Nishitani, Y. Shirai, M. Yamaguchi, Deformation of polysynthetically twinned crystals of TiAl with a nearly stoichiometric composition, Philos. Mag. A 61 (4) (1990) 591–606.
[4] H. Inui, M.H. Oh, A. Nakamura, M. Yamaguchi, Room-temperature tensile deformation of polysynthetically twinned (PST) crystals of TiAl, Acta Metall. Mater. 40 (11) (1992) 3095–3104.
[5] R. Lebensohn, H. Uhlenhut, C. Hartig, H. Mecking, Plastic flow of γ-TiAl-based polysynthetically twinned crystals: micromechanical modeling and experimental validation, Acta Mater. 46 (13) (1998) 4701–4709.
[6] T.E.J. Edwards, F. Di Gioacchino, R. Muñoz-Moreno, W.J. Clegg, Deformation of lamellar TiAl alloys by longitudinal twinning, Scr. Mater. 118 (2016) 46–50.
[7] H.Y. Kim, K. Maruyama, Parallel twinning during creep deformation in soft orientation PST crystal of TiAl alloy, Acta Mater. 49 (14) (2001) 2635–2643.
[8] R. Muñoz-Moreno, M.T. Pérez-Prado, J. Llorca, E.M. Ruiz-Navas, C.J. Boehlert, Effect of stress level on the high temperature deformation and fracture mechanisms of Ti-45Al-2Nb-2Mn-0.8 vol. pct TiB_2: an in situ experimental study, Metall Mat Trans A 44 (4) (2013) 1887–1896.
[9] C. Içöz, L. Patriarca, M. Filippini, S. Beretta, Strain accumulation in TiAl intermetallics via high-resolution digital image correlation (DIC), Procedia Eng. 74 (0) (2014) 443–448.
[10] B.A. Simkin, B.C. Ng, M.A. Crimp, T.R. Bieler, Crack opening due to deformation twin shear at grain boundaries in near-γ TiAl, Intermetallics 15 (1) (2007) 55–60.
[11] K. Thomsen, N.H. Schmidt, A. Bewick, K. Larsen, J. Goulden, Improving the accuracy of orientation measurements using EBSD, Microsc. Microanal. 19 (S2) (2013) 724–725.
[12] D.E. Larsen, S. Kampe, L. Christodoulou, Effect of XD™ TiB2 volume fraction on the microstructure of a cast near-gamma titanium aluminide alloy, MRS Online Proc. Libr. 194 (1990) null-null.
[13] D. Hu, Role of boron in TiAl alloy development: a review, Rare Met. 35 (1) (2015) 1–14.
[14] W.J. Zhang, S.C. Deevi, An analysis of the lamellar transformation in TiAl alloys containing boron, Mater. Sci. Eng. A 337 (1–2) (2002) 17–20.
[15] C.L. Chen, W. Lu, J.P. Lin, L.L. He, G.L. Chen, H.Q. Ye, Orientation relationship between TiB precipitate and γ-TiAl phase, Scr. Mater. 56 (6) (2007) 441–444.
[16] Standard Test Method for Analysis of Titanium and Titanium Alloys by Direct Current Plasma and Inductively Coupled Plasma Atomic Emission Spectrometry (Performance-based Test Methodology), ASTM International, 2013.
[17] Standard Test Method for Determination of Oxygen and Nitrogen in Titanium and Titanium Alloys by Inert Gas Fusion, ASTM International, 2013.
[18] Standard Test Method for Determination of Carbon in Refractory and Reactive Metals and Their Alloys by Combustion Analysis, ASTM International, 2016.
[19] Standard Test Method for Determination of Hydrogen in Titanium and Titanium Alloys by Inert Gas Fusion Thermal Conductivity/infrared Detection Method, ASTM International, 2016.
[20] A.S.T.M. International, E 112 Standard Test Methods for Determining Average Grain Size, 2004.
[21] T.E.J. Edwards, F. Di Gioacchino, H.P. Springbett, R.A. Oliver, W.J. Clegg, Stable speckle patterns for nano-scale strain mapping up to 700 °C, Exp. Mech. (2017), http://dx.doi.org/10.1007/s11340-017-0317-8.
[22] K. Fujimura, K. Kishida, K. Tanaka, H. Inui, Compression of micropillars of TiAl coexisting with Ti3Al, MRS Online Proc. Libr. 1295 (2011) 201–206.
[23] Y. Umakoshi, T. Nakano, The role of ordered domains and slip mode of α2 phase in the plastic behaviour of TiAl crystals containing oriented lamellae, Acta Metall. Mater. 41 (4) (1993) 1155–1161.
[24] B.K. Kad, R.J. Asaro, Apparent Hall-Petch effects in polycrystalline lamellar TiAl, Philos. Mag. A 75 (1) (1997) 87–104.
[25] S.K. Jha, J.M. Larsen, A.H. Rosenberger, The role of competing mechanisms in the fatigue life variability of a nearly fully-lamellar γ-TiAl based alloy, Acta Mater. 53 (5) (2005) 1293–1304.
[26] F. Appel, U. Brossmann, U. Christoph, S. Eggert, P. Janschek, U. Lorenz, J. Müllauer, M. Oehring, J.D.H. Paul, Recent progress in the development of gamma titanium aluminide alloys, Adv. Eng. Mater. 2 (11) (2000) 699–720.
[27] Y. Umakoshi, H.Y. Yasuda, T. Nakano, Plastic anisotropy and fatigue of TiAl PST crystals: a review, Intermetallics 4 (1) (1996) S65–S75.
[28] J.W. Christian, S. Mahajan, Deformation twinning, Prog. Mater. Sci. 39 (1–2) (1995) 1–157.
[29] T. Leitner, M. Schloffer, S. Mayer, J. Eßlinger, H. Clemens, R. Pippan, Fracture and R-curve behavior of an intermetallic β-stabilized TiAl alloy with different nearly lamellar microstructures, Intermetallics 53 (2014) 1–9.
[30] J.F. Nye, Some geometrical relations in dislocated crystals, Acta metall. 1 (2) (1953) 153–162.
[31] G. Cao, L. Fu, J. Lin, Y. Zhang, C. Chen, The relationships of microstructure and properties of a fully lamellar TiAl alloy, Intermetallics 8 (5–6) (2000) 647–653.
[32] D. Hu, A. Huang, H. Jiang, N. Mota-Solis, X. Wu, Pre-yielding and pre-yield cracking in TiAl-based alloys, Intermetallics 14 (1) (2006) 82–90.
[33] J.P. Campbell, J.J. Kruzic, S. Lillibridge, K.T.V. Rao, R.O. Ritchie, On the growth of small fatigue cracks in γ-based titanium aluminides, Scr. Mater. 37 (5) (1997) 707–712.